# Theoretical study of the dynamics, stereodynamics, and microscopic mechanism of the $O(^1D)+CH_4(X\,^1A_1)\rightarrow OH(X\,^2\Pi)+CH_3(X\,^2A_2'')$ reaction

Miguel González[a] and Jordi Hernando
*Departament de Química Física i Centre de Recerca en Química Teòrica, Universitat de Barcelona. C/ Martí i Franquès, 1. 08028 Barcelona, Spain*

María P. Puyuelo
*Departamento de Química, Universidad de La Rioja, C/ Obispo Bustamante, 3. 26004 Logroño, Spain*

R. Sayós[a]
*Departament de Química Física i Centre de Recerca en Química Teòrica, Universitat de Barcelona, C/ Martí i Franquès, 1. 08028 Barcelona, Spain*

(Received 15 February 2000; accepted 5 July 2000)

A previously reported potential energy surface (PES) and a new barrierless PES (both based on *ab initio* data and describing the $CH_3$ group as a pseudoatom) were used to study the $O(^1D)+CH_4\rightarrow OH+CH_3$ reaction with the quasiclassical trajectory (QCT) method. The new PES accurately reproduces the experimental rate constant values, in contrast to the previous PES. The QCT study was mainly performed at the relative translational energy ($E_T$) resulting from the photodissociation of $N_2O$ at 193 nm ($\langle E_T\rangle=0.403$ eV), although the collision energy obtained from the photodissociation of $O_3$ at 248 nm ($\langle E_T\rangle=0.212$ eV) was also considered. Good agreement between theory and experiment was obtained for the OH vibrational populations and for the OH rotational populations for the $v'\geqslant 2$ vibrational levels, while the rotational distributions for $v'=0-1$ are more excited than in the experiment. The QCT results at $E_T=0.403$ eV satisfactorily reproduce the experimental $\mathbf{kk}'$ angular distribution of the state-specific channel OH($v'=4$, $N'=8$) and the corresponding $E_T'$ distribution. For OH($v'=0$, $N'=5$) the reproduction of these properties is poorer, especially for the $E_T'$ distribution. At 0.403 eV the contribution of the abstraction mechanism to the reaction mode is negligible and two insertion like mechanisms (with fast or slow elimination) are found to be predominant, as suggested experimentally. The discrepancies observed between the QCT and experimental results can be explained on the basis of the defective description of the insertion/slow elimination mechanism provided by the model. © *2000 American Institute of Physics.* [S0021-9606(00)00437-2]

## I. INTRODUCTION

The reaction of the oxygen atom in the first excited electronic state, $O(^1D)$, with the most abundant hydrocarbon in the atmosphere, $CH_4$, is an important source of stratospheric OH, which is involved in the natural degradation processes of the ozone layer through the OH–$HO_2$ catalytic cycle.[1–3] In addition to the relevance of this reaction in stratospheric chemistry, the different reactive behavior of the $O(^1D)$ atom with respect to that of the ground-state oxygen atom, $O(^3P)$, makes the study of the gas-phase reaction

$$O(^1D)+CH_4(X^1A_1)\rightarrow OH(X^2\Pi)+CH_3(X^2A_2'')$$

$$\Delta H^o_{298\,K}=-43.1\ \text{kcal mol}^{-1},^4 \qquad (1)$$

of great interest in chemical dynamics.

The $O(^1D)+CH_4$ reaction was extensively studied using several experimental techniques. The global, including all possible reaction channels, thermal rate constant for this reaction is very large ($1.5\times10^{-10}$ $\text{cm}^3\,\text{molecule}^{-1}\,\text{s}^{-1}$ for $T=200-350$ K[5]) and approaches the gas kinetic limit value. This suggests that the reaction does not present activation energy, in contrast to the analogous reaction with $O(^3P)$.[6] In a recent contribution,[7] in which the authors used their own data obtained from crossed-beam experiments and results from other researchers,[8–11] the following product branching ratios for the $O(^1D)+CH_4$ reaction were recommended: $\Phi(OH(X^2\Pi)+CH_3(X^2A_2''))=0.69$, $\Phi(CH_2OH(X^2A_1)/CH_3O(X^2A')+H(^2S))=0.23$, $\Phi(CH_2O(X^1A_1)+H_2(X^1\Sigma_g^+)/CH_2O(X^1A_1)+2H(^2S))=0.05$, $\Phi(CH_2(a^1A_1)+H_2O(X^1A_1))=0.015$, and $\Phi(O(^3P)+CH_4(X^1A_1))=0.015$.

The measurement of the nascent $OH(X^2\Pi)$ vibrational[12–19] and rotational[12,15–19] distributions arising from reaction (1) was the object of several studies, mainly using laser- induced fluorescence (LIF) to probe this radical. The $O(^1D)$ atoms were generated by photodissociation of $N_2O$ (193 nm) or $O_3$ (248 or 266 nm), allowing the authors to study the effect of the $O(^1D)+CH_4$ collision energy (relative translational energy, $E_T$) on the $OH(X^2\Pi)$ product energy distribution. The energy distributions found experimentally seem to be slightly dependent on $E_T$, probably because the reaction is highly exothermic which attenuates the influence of the initial reaction conditions on the dynamics. $\langle E_T\rangle$

[a]Authors to whom correspondence should be addressed. Electronic mail: miguel@qf.ub.es, r.sayos@qf.ub.es

 © 2000 American Institute of Physics

is 0.403 and 0.212 eV for the reactions photoinitiated by photolysis of $N_2O$ (193 nm) and $O_3$ (248 nm), respectively, and the energy available in products is 2.30 and 2.11 eV, respectively. Vibrational populated levels up to $v'=4$ with a relatively flat vibrational distribution for $v'=0-3$ were determined.[13–15] A bimodal rotational distribution was observed essentially for $v'=0$, which was assumed to be due to two different microscopic reaction mechanisms.[12,15–19] The $OH(X\,^2\Pi_{3/2})/OH(X\,^2\Pi_{1/2})$ spin–orbit population ratio is statistical[12,15–19] and the $\Pi(A')/\Pi(A'')$ lambda doublet population ratio is greater than one.[12,15,16,18,19] Both features are in contrast to what happens for the analogous reaction with $O(^3P)$. The energy distributions of the OH product arising from the photolysis of $O_3 \bullet CH_4$ clusters at 267,[20] or 266 and 267 nm,[21] and $N_2O \bullet CH_4$ clusters at 193 nm[18] were also reported. Furthermore, polarized Doppler-resolved LIF spectroscopy[22–26] was used to study the stereodynamics of reaction (1). Both the $OH(v'=0,\ N'=5,\ 8)$ and $OH(v'=4,\ N'=8)$ $\mathbf{kk}'$ differential cross sections (DCS) exhibit forward and backward peaks, the backward peak for $OH(v'=0,\ N'=5,\ 8)$ and the forward peak for $OH(v'=4,\ N'=8)$ being slightly dominant.

The energy distribution of the $CH_3$ molecules produced in reaction (1) was also measured.[27,28] The ''umbrella'' mode ($\nu_2$) and the symmetric stretch ($\nu_1$) nascent vibrational populations are noninverted, and the $\nu_2$ mode is much colder than the unconstrained statistical populations. The rotational distribution[28] is much hotter than at room temperature.

Some experimental studies have attempted to elucidate the microscopic mechanism of reaction (1) and the analogous half collision reaction. A lifetime of about 0.8 ps was obtained for a long-lived $CH_3OH$ intermediate, through which about half the total $CH_3$ and OH molecules produced from the bimolecular reaction were found to evolve.[29] In this experiment, however, it was not determined whether the $O(^1D)$ was thermalized before reaction. A lifetime of about 3 ps for the $CH_3OH$ intermediate was measured for the photoinitiated reaction through the $O_3 \bullet CH_4$ cluster[20] and, more recently, three independent temporal components were found in the OH rate of formation for the same photolyzed van der Waals complex.[21] These three components are believed to correspond to three microscopic reaction mechanisms.

From a theoretical point of view, an *ab initio* study at the CCI//CASSCF (contracted configuration interaction// complete active space self-consistent field) level on the $CH_2+H_2O$, $HCOH+H_2$, and $CH_2O+H_2$ reaction channels,[30] and an *ab initio* study at the MRCI//CASSCF level focused on the description of the reaction path which connects reactants with the $CH_3OH$ alcohol intermediate and the $OH+CH_3$ and $CH_3O+H$ products[31] were reported. Recently, we have performed an *ab initio* study at the PUMP4//UMP2 (spin-projected unrestricted fourth-order Møller–Plesset perturbational method considering the geometry obtained at the unrestricted second-order Møller–Plesset perturbational method) level of the ground potential-energy surface (PES) of reaction (1).[32] In the same study a triatomic analytical representation of this PES was derived from the *ab initio* data, considering the $CH_3$ group as a pseudoatom of 15 amu. The reliability of this model was checked by comparing the OH energy distribution calculated by the quasiclassical trajectory (QCT) method at $E_T=0.212$ eV with the experimental distribution.[13,15] A quite good agreement was found between the calculated and experimental OH energy distributions. Similar results were also achieved in QCT preliminary calculations carried out on the same analytical PES at $E_T=0.403$ eV.[19] However, the neglect of the internal degrees of freedom of the $CH_3$ fragment assumed in the triatomic PES model results in the appearence of an energy barrier along the minimum energy path, which contrasts with the experimental evidence that this reaction exhibits no activation energy. To deal with this problem, in the present contribution a barrierless triatomic analytical PES was derived for the $O(^1D)+CH_4$ system. This new PES and that described in Ref. 32 were used here to study the dynamics, stereodynamics and microscopic mechanism of the $O(^1D)+CH_4(X\,^1A_1)\rightarrow OH(X\,^2\Pi)+CH_3(X\,^2A_2'')$ reaction by the QCT method.

This paper is organized as follows: Section II deals with the analytical PES and Sec. III considers the QCT study (rate constants, rovibrational distributions, stereodynamics, and microscopic reaction mechanism). Finally, the summary and conclusions are given in Sec. IV.

## II. POTENTIAL ENERGY SURFACE

For $C_1$, $C_s$ and $C_{3v}$ symmetries, the following PES correlate adiabatically with both asymptotic regions of reaction (1): (2) $^1A$ ($C_1$), $^1A'+{}^1A''$ ($C_s$) and $^1E$ ($C_{3v}$). In a previous study by our group,[32] the ground PES ($^1A'$ in $C_s$ symmetry) of the $O(^1D)+CH_4$ system was characterized at the PUMP4//UMP2 Møller–Plesset *ab initio* level with the 6-311G(2*df*, 2*pd*) basis set. A total of 126 *ab initio* points (geometries and energies) were calculated to describe reactants, the $OH+CH_3$ and $CH_3O+H$ products, the $CH_3OH$ alcohol minimum, the $OHCH_3$ saddle point, the reaction paths connecting all these stationary points, and additional points in other regions of interest. The minimum energy path (MEP) found for reaction (1) follows a collinear approach of the $O(^1D)$ atom to the H–$CH_3$ bond until the saddle point structure is reached. When the UMP2 zero-point energy (ZPE) is included the energy of the saddle point falls below the $O(^1D)+CH_4$ asymptote (0.1 kcal mol$^{-1}$ below the energy of reactants, while it is 3.6 kcal mol$^{-1}$ above reactants when the ZPE is not accounted for). This suggests that after inclusion of the ZPE there is no barrier for reaction (1), as also suggested experimentally[5] and in a previous *ab initio* calculation.[31] The MEP after the saddle point structure leads directly to the formation of the $OH+CH_3$ products, although the insertion of the $O(^1D)$ atom into the C–H bond to yield the $CH_3OH$ minimum can easily be achieved thanks to the O–H–$CH_3$ bending motion. Once the minimum is formed, it can lead to $OH+CH_3$ or $CH_3O+H$ without any barrier over products.

From these *ab initio* data, a triatomic model was developed by us in a previous contribution[32], where the $CH_3$ fragment was treated as a single atom of 15 amu placed in its center of mass, to construct an analytical representation of the ground PES for reaction (1). This model only accounts

TABLE I. Optimal parameters for the analytical triatomic PES2.

| *Two-body terms:* Species | $D_e$/eV | $R_e$/Å | $a_1$/Å$^{-1}$ | $a_2$/Å$^{-2}$ | $a_3$/Å$^{-3}$ |
|---|---|---|---|---|---|
| O–H[a] | 6.4659 | 0.9634 | 3.8782 | 3.6827 | 5.2431 |
| H–($CH_3$) | 4.7922 | 1.1566 | 4.1842 | 5.2347 | 4.7665 |
| O–($CH_3$)[a] | 5.7931 | 1.4444 | 4.4502 | 7.0280 | 9.8229 |
| *Three-body term:*[b] | | | | | |
| $c_{000}$ | 4.7034 | $c_{300}$ | 1.6628 | $\gamma_1$ | 1.3754 |
| $c_{100}$ | 1.5556 | $c_{210}$ | 2.3619 | | |
| $c_{010}$ | −4.5083 | $c_{201}$ | −2.4838 | $\gamma_2$ | 1.9066 |
| $c_{001}$ | 1.6639 | $c_{120}$ | −9.6673 | | |
| $c_{200}$ | 1.3504 | $c_{111}$ | −5.0630 | $\gamma_3$ | 1.8564 |
| $c_{110}$ | −0.355 52 | $c_{102}$ | −1.9042 | | |
| $c_{101}$ | −5.2946 | $c_{030}$ | 3.5840 | | |
| $c_{020}$ | −0.298 41 | $c_{021}$ | −5.8580 | $R^0_{OH}$ | 1.2345 |
| $c_{011}$ | −1.6461 | $c_{012}$ | −3.4669 | $R^0_{H-(CH3)}$ | 1.6037 |
| $c_{002}$ | 3.7913 | $c_{003}$ | 1.5833 | $R^0_{O-(CH3)}$ | 2.1053 |

[a]The dissociation energies of O–H and O–($CH_3$) are given with respect to O($^1D$)+H and O($^1D$)+($CH_3$), respectively, although their true dissociation limits are O($^3P$)+H and O($^3P$)+($CH_3$), respectively. This has been done to preserve the same dissociation limits in the three asymptotic regions of the analytical PES. See also Ref. 32.
[b]Units are: $c_{ijk}$/eV Å$^{-(i+j+k)}$, $\gamma_i$/Å$^{-1}$, $R_i$/Å.

for two ($OH+CH_3$ and $CH_3O+H$) of the possible reaction channels available for O($^1D$)+$CH_4$. However, as under thermal conditions the $OH+CH_3$ channel is clearly the main one ($\Phi=0.69$) and $\Phi(CH_2OH/CH_3+H)=0.23$,[7] the triatomic model proposed appears to be a reasonable starting point to describe this polyatomic system. This was confirmed in previous QCT studies carried out by our group on reaction (1).[19,32]

The same type of analytical expression[33] (many-body expansion) used in previous studies of our group (O($^3P$)+H($CH_3$),[6] N+NO,[34] O($^3P$)+CS,[35] H+$Cl_2$,[36] N+$O_2$,[37] and H+ClF[38]) was also used[32] to describe the PES of reaction (1):

$$V(R_1,R_2,R_3)=V^{(2)}_{OH}(R_1)+V^{(2)}_{H(CH_3)}(R_2)+V^{(2)}_{O(CH_3)}(R_3)+V^{(3)}_{OH(CH_3)}(R_1,R_2,R_3), \quad (2)$$

where $R_1$, $R_2$, $R_3$ are the O–H, H–($CH_3$) and O–($CH_3$) distances, and $V^{(2)}$ and $V^{(3)}$ are, respectively, the two-body (extended-Rydberg potential up to third order) and three-body (product of a third- order polynomial and a range function) terms, which are given by:

$$V^{(2)}(\rho)=-D_e(1+a_1\rho+a_2\rho^2+a_3\rho^3)e^{-a_1\rho}, \quad (3)$$

$$V^{(3)}_{OH(CH_3)}(\rho_1,\rho_2,\rho_3)=\sum_{i,j,k=0}^{0\leq i+j+k\leq 3} c_{ijk}\rho_1^i\rho_2^j\rho_3^k \times\prod_{i=1}^{3}\left[1-\tanh\left(\frac{\gamma_i\rho_i}{2}\right)\right], \quad (4)$$

where $D_e$ and $R_e$ are equal to the dissociation energy and equilibrium bond length of the corresponding diatomic molecule, respectively, $\rho$ and $\rho_i$ are defined as $R-R_e$, and $R_i-R_i^o$, respectively, where ($R_1^o$, $R_2^o$, $R_3^o$) is a selected triatomic reference structure, and $a_i$, $c_{ijk}$, and $\gamma_i$ are parameters to be optimized. The optimal parameters obtained by fitting the *ab initio* data using the expressions indicated above were reported elsewhere.[32] The resulting analytical PES (PES1 hereafter) accurately reproduced the *ab initio* information, and in particular the reaction exoergicity, and the $CH_3OH$ minimum and saddle point energies. However, this agreement was poorer when the ZPE was included, due to the neglect of the internal degrees of freedom of the methyl fragment in the triatomic model. This was also observed in previous triatomic models (see, e.g., Ref. 6). Thus, while after inclusion of the ZPE there was no barrier from the *ab initio* data, for PES1 a barrier of 2.2 kcal mol$^{-1}$ was found (4.1 kcal mol$^{-1}$ without ZPE). As proved in a subsequent QCT calculation,[32] the barrier on PES1 led to a QCT excitation function which showed opposite behavior to that expected for a barrierless reaction: The cross section of reaction (1) increases with $E_T$ instead of decreasing. Of course, as classical trajectories are propagated without considering the ZPE, it is the barrier on the PES that affects the QCT results.

The same type of many-body expansion [Eqs. (2)–(4)] and programs[39,40] considered to derive PES1 were used here to construct a new analytical triatomic representation of the ground PES of reaction (1) that does not present an energy barrier along the MEP even if the ZPE is considered. To obtain the new PES, 104 of the 126 available *ab initio* points were fitted without restriction. The energies of the saddle point and points connecting reactants with the saddle point were taken as equal to the energy of reactants (11 points), and the energies of the *ab initio* points describing the bending of the O–H–($CH_3$) saddle point structure (11 points) have been shifted according to the energy shift applied to the saddle point energy. The reliability of the resulting analytical PES (about 20) has been checked by comparing the QCT calculated rate constant with the experimental value at 300 K.[5] The barrierless analytical PES which best reproduced this property (PES2 hereafter) was chosen to study reaction (1). The optimal parameters of PES2 are given in Table I.

On the other hand, PES2 accurately reproduces the *ab initio* information about the minimum, the exit channels and other regions explored. Thus, e.g., the geometry of the $CH_3OH$ minimum on PES2 ($R_{OH}=0.9534$ Å, $R_{H(CH3)}=1.9846$ Å and $\angle$O–H–($CH_3$)$=46.2°$) shows good agreement with the *ab initio* data ($R_{OH}=0.9560$ Å, $R_{H(CH3)}=1.9992$ Å and $\angle$O–H–($CH_3$)$=45.2°$). Agreement is also found when the fitted energies (−127.8 and −132.6 kcal mol$^{-1}$, respectively, with and without ZPE) and *ab initio* energies (−129.2 and −133.5 kcal mol$^{-1}$, respectively, with and without ZPE) of the minimum are compared.

## III. QCT STUDY

To study reaction (1) the QCT method,[41–43] as implemented in the TRIQCT program,[44] was employed using the analytical PES1 and PES2 expressions. As already mentioned, the former PES presents a spurious barrier. Nevertheless, PES1 was also used here as the QCT OH rovibrational populations previously obtained by us[19,32] from this PES [$E_T=0.212$ and 0.403 eV with H–($CH_3$) ($T=298$ K)] reproduce quite well the experimental data. The accuracy of the

TABLE II. Global rate constant ($k$) and branching ratio ($k_1/k$) for the $O(^1D)+CH_4$ system.[a]

| | $k$/cm$^3$ molecule$^{-1}$ s$^{-1}$ | | | | |
|---|---|---|---|---|---|
| Study | $T=200$ K | $T=250$ K | $T=300$ K | $T=350$ K | $k_1/k$ branching ratio |
| QCT PES2 | $(1.69\pm0.03)\times10^{-10}$ | $(1.60\pm0.03)\times10^{-10}$ | $(1.53\pm0.03)\times10^{-10}$ | $(1.50\pm0.03)\times10^{-10}$ | $0.68\pm0.03$[a] |
| Exp.[b] | $1.5\times10^{-10}$ | $1.5\times10^{-10}$ | $1.5\times10^{-10}$ | $1.5\times10^{-10}$ | $0.75\pm0.15$ |
| Exp.[c] | | | | | 0.69 |

[a]Branching ratio value at 300 K. The values at $T=200$, 250, and 350 K are, respectively, 0.69, 0.69, and 0.66. QCT errors correspond to one standard deviation.
[b]Reference 5. The error in $k$ is equal to $(+0.4, -0.3)\times10^{-10}$ cm$^3$ molecule $^{-1}$ s$^{-1}$ and the branching ratio is given at 298 K.
[c]Reference 7. Branching ratio at room temperature.

numerical integration of Hamilton's differential equations was verified by checking the conservation of total energy and total angular momentum along every trajectory, and performing back-integrations on some batches of trajectories. An integration step of $0.25\times10^{-16}$ s and an initial distance of 10 Å between the $O(^1D)$ and the H–($CH_3$) center of mass were selected. This separation ensures that the interaction energy can be neglected with respect to the available energy of reactants.

To calculate the QCT rate constant values (Sec. III A), both $E_T$ and the rovibrational distribution of the H–($CH_3$) molecule were sampled from the corresponding Maxwell–Boltzmann distributions ($T=200$, 250, 300, and 350 K), and around 15 000 trajectories were calculated at each temperature. To study the OH rovibrational distributions (Sec. III B) and the stereodynamics (Sec. III C), the rovibrational distribution of the H–($CH_3$) pseudodiatomic molecule was sampled from a Maxwell–Boltzmann distribution at 298 K and several $E_T$ values were considered. For each initial collision energy studied, around 300 000 trajectories were calculated. Moreover, to compare the QCT rotational populations with the experimental data, as the QCT method does not include either the orbital ($\Lambda=1$) or the spin ($S=1/2$) electronic angular momenta of the $OH(X\,^2\Pi)$ molecule, we have assumed $N'$, the total angular momentum quantum number (excluding the electronic and nuclear spins), to be equal to $j'$, the rotational angular momentum quantum number, plus one.

### A. Rate constants

A crude estimation [as there is a deep minimum between reactants and products that can easily be reached (cf. Sec. III D)] of the rate constant value of reaction (1) at 300 K can be obtained from the transition state theory (TST). Thus, an improved canonical variational transition state theory (ICVT) calculation with microcanonical optimized multidimensional tunneling (ICVT/$\mu$OMT method hereafter) of the rate constant at 300 K for PES1 using the POLYRATE program[45] gives a value of $3.5\times10^{-13}$ cm$^3$ molecule$^{-1}$ s$^{-1}$, which is much lower than the experimental result ($1.1\times10^{-10}$ cm$^3$ molecule$^{-1}$ s$^{-1}$).[5] This is due to the spurious barrier that is present in the PES1 analytical representation once the ZPE is included. On the other hand, a simple TST calculation using directly the *ab initio* energy, geometry and harmonic frequencies of the saddle point and reactants leads to a rate constant of $0.8\times10^{-10}$ cm$^3$ molecule$^{-1}$ s$^{-1}$, reasonably close to the experimental value.

As indicated, PES2 was fitted taking into account that the PES should not present any barrier above reactants. The QCT global rate constant (including all the possible channels) and branching ratio values from PES2 at 200, 250, 300, and 350 K are compared with the experimental data in Table II. A quite good agreement between the QCT and experimental global rate constants can be observed. Thus, as found experimentally, the QCT global rate constant also shows a weak dependence on the temperature. A satisfactory agreement is also obtained between the QCT and experimental branching ratios for the main channel ($OH+CH_3$), although it should emphasized that the triatomic model is only able to account for two possible reaction channels ($OH+CH_3$ and $CH_3O+H$). The dependence on $E_T$ of the branching ratio for the $OH+CH_3$ channel was also analyzed, obtaining a decrease of the branching ratio value as $E_T$ increases. The ratio evolves from 0.67 to 0.60 as $E_T$ increases from 0.1 to 1.0 eV. Similar results with a greater influence of $E_T$ on the branching ratio were reported in our previous contribution on PES1.[32] In that case the change of $E_T$ from 0.212 to 0.8 eV resulted in a decrease of the branching ratio from 0.66 to 0.48.

In all the kinetics calculations, to account for the fact that there are four equivalent hydrogen atoms in the methane molecule, and assuming that the reaction channel involving each hydrogen atom is independent, the calculated rate constant values derived from the ground $^1A'$ PES were multiplied by four (statistical factor). Furthermore, as there are five adiabatic PES correlating with the reactants asymptote ($(3)\,^1A'+(2)\,^1A''$ in $C_s$ symmetry), the calculated rate constant values were also divided by five to obtain the rate constant of the system. The rotational symmetry numbers were considered as equal to 1 in the case of the transition state theory calculations.

### B. Rovibrational distributions

In our previous contributions on reaction (1),[19,32] the QCT calculations of the $OH(X\,^2\Pi)$ rovibrational distributions were performed using PES1, considering the two average $E_T$ values of the $O(^1D)+CH_4$ system which result when the $O(^1D)$ is generated by photodissociation of $O_3$ at 248 nm ($\langle E_T\rangle=0.212$ eV) and of $N_2O$ at 193 nm ($\langle E_T\rangle=0.403$ eV). The most reliable experimental studies on the OH rovibrational distributions [Refs. 13 and 15 ($O_3$, 248 nm) and Refs. 17–19 ($N_2O$, 193 nm)] were carried out using both photodissociation processes.

TABLE III. Vibrational populations and average rotational levels of OH($X^2\Pi$) arising from $O(^1D)+CH_4 \rightarrow OH+CH_3$ reaction.

| | | $P(v')/P(v'=1)$ and $\langle N' \rangle_{v'}$[a] | | | | | | |
|---|---|---|---|---|---|---|---|---|
| Methodology | $E_T$/eV | $v'=0$ | $v'=1$ | $v'=2$ | $v'=3$ | $v'=4$ | $v'=5$ | $v'=6$ |
| QCT PES1 | 0.212[b] | 0.97±0.03 | 1.00±0.03 | 1.09±0.03 | 0.98±0.03 | 0.48±0.02 | | |
| | | (14.4±0.3) | (13.2±0.2) | (12.5±0.2) | (10.1±0.2) | (6.8±0.2) | | |
| | 0.403 | 1.16±0.02 | 1.00±0.02 | 1.00±0.02 | 0.85±0.02 | 0.47±0.01 | 0.07±0.01 | |
| | | (17.0±0.3) | (16.4±0.2) | (15.0±0.2) | (13.3±0.2) | (10.0±0.2) | (5.6±0.3) | |
| | $f(E_T)O(^1D)_{N_2O-193\ nm}$ | 1.12±0.02 | 1.00±0.02 | 0.96±0.02 | 0.86±0.02 | 0.53±0.02 | 0.10±0.01 | 0.005±0.001 |
| | | (17.5±0.3) | (16.7±0.3) | (15.5±0.3) | (13.7±0.2) | (10.9±0.3) | (7.5±0.3) | (6.1±1.7) |
| QCT PES2 | 0.212 | 1.04±0.03 | 1.00±0.03 | 0.91±0.03 | 0.71±0.03 | 0.30±0.01 | | |
| | | (18.3±0.3) | (16.6±0.3) | (13.8±0.3) | (11.1±0.2) | (7.2±0.2) | | |
| | 0.403 | 1.12±0.02 | 1.00±0.02 | 0.84±0.02 | 0.72±0.02 | 0.41±0.01 | 0.05±0.01 | |
| | | (19.9±0.2) | (18.2±0.2) | (15.5±0.2) | (12.7±0.2) | (9.3±0.2) | (5.3±0.3) | |
| | $f(E_T)O(^1D)_{N_2O-193\ nm}$ | 1.09±0.03 | 1.00±0.03 | 0.88±0.02 | 0.71±0.02 | 0.43±0.01 | 0.08±0.01 | 0.004±0.001 |
| | | (19.6±0.3) | (17.9±0.3) | (15.3±0.3) | (12.5±0.3) | (9.5±0.3) | (6.6±0.4) | (6.0±1.8) |
| Exp.[c] | $f(E_T)O(^1D)_{O_3-248\ nm}$ | | 1.00 | 1.22 | 0.97 | 0.52 | | |
| Exp.[d] | $f(E_T)O(^1D)_{O_3-248\ nm}$ | 1.00 | 1.00 | 1.32 | 0.47 | 0.19 | | |
| | | (13.6) | (12.8) | (12.4) | (8.8) | (6.4) | | |
| Exp.[e] | $f(E_T)O(^1D)_{N_2O-193\ nm}$ | 0.92 | 1.00 | | | | | |
| Exp.[f] | $f(E_T)O(^1D)_{N_2O-193\ nm}$ | 1.44±0.38 | 1.00 | | | | | |
| | | (12.7±0.3) | (12.7±0.4) | | | | | |

[a]The first value given corresponds to the $P(v')/P(v'=1)$ ratio and the second one appearing in parentheses is the average rotational level. QCT errors correspond to one standard deviation. The $b_{max}$ and reaction probability values are the following: (a) 2.55 Å and 0.14 (0.403 eV) and 2.68 Å and 0.11 ($f(E_T)$) for PES1; (b) 3.71 Å and 0.23 (0.403 eV) and 5.16 Å and 0.14 ($f(E_T)$) for PES2.
[b]Reference 32.
[c]Reference 13.
[d]Reference 15.
[e]Reference 18.
[f]Reference 19.

Here, these two initial collision energies were also considered in the QCT calculations on PES2, and the statistics of the calculations on PES1 at $E_T=0.403$ eV reported in Ref. 19 was improved. Furthermore, as the nascent translational energy distribution of the $O(^1D)-N_2$ pair arising from the photodissociation of $N_2O$ at 193 nm was measured,[46,47] additional QCT calculations were performed on both PES in a more rigorous way, taking into account the $O(^1D)+CH_4$ $E_T$ distribution ($f(E_T)$ hereafter) associated with the $O(^1D)$ generation from $N_2O$ at 193 nm.[46]

The QCT OH vibrational distributions and average rotational levels obtained at $E_T=0.212$, 0.403 eV and $f(E_T)$ for PES1 and PES2 are given in Table III, along with the experimental data.[13,15,18,19] The QCT ($v'=0-5$) vibrational and rotational distributions at $E_T=0.403$ eV and $f(E_T)$ are plotted in Figs. 1 and 2, respectively, together with the measured data ($v'=0-1$).

As reported in Ref. 32, a quite good agreement was found between the experimental[13,15] and QCT vibrational and rotational (especially for $v'=2-4$) distributions calculated on PES1 at $E_T=0.212$ eV. The results obtained with the barrierless PES2 at this $E_T$ value are similar to those obtained in the previous calculations on PES1 (Table III). However, PES2 leads to less vibrational excitation and more rotational excitation (particularly for $v'=0-1$) of the OH($X^2\Pi$) product than PES1. The largest difference between the two PES appears when the rotational distributions for $v'=0-1$ are compared. The vibrational distribution obtained for PES2 is quite flat for $v'=0-2$, reaches vibrational levels up to $v'=4$ and shows a maximum at $v'=0$. The vibrational distributions obtained for PES1 and from the experiments are also quite flat for $v'=0-2$ but peak at $v'=2$.

In the QCT calculations simulating the $O(^1D)+CH_4$ reaction photoinitiated from $N_2O$ at 193 nm, in general almost negligible differences are observed when either the average $E_T$ value ($E_T=0.403$ eV) or the full $E_T$ distribution of reac-

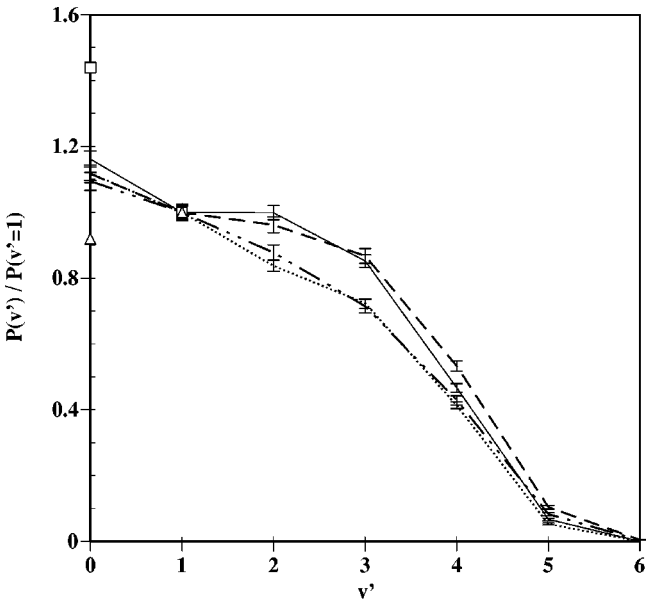


FIG. 1. QCT [—- PES1–0.403 eV, – – PES1-$f(E_T)$, ··· PES2–0.403 eV, and —·-·— PES2-$f(E_T)$] and experimental (△, Ref. 18 and □, Ref. 19) OH($X^2\Pi$) vibrational distributions arising from reaction (1) with $O(^1D)$ generated by photodissociation of $N_2O$ at 193 nm.

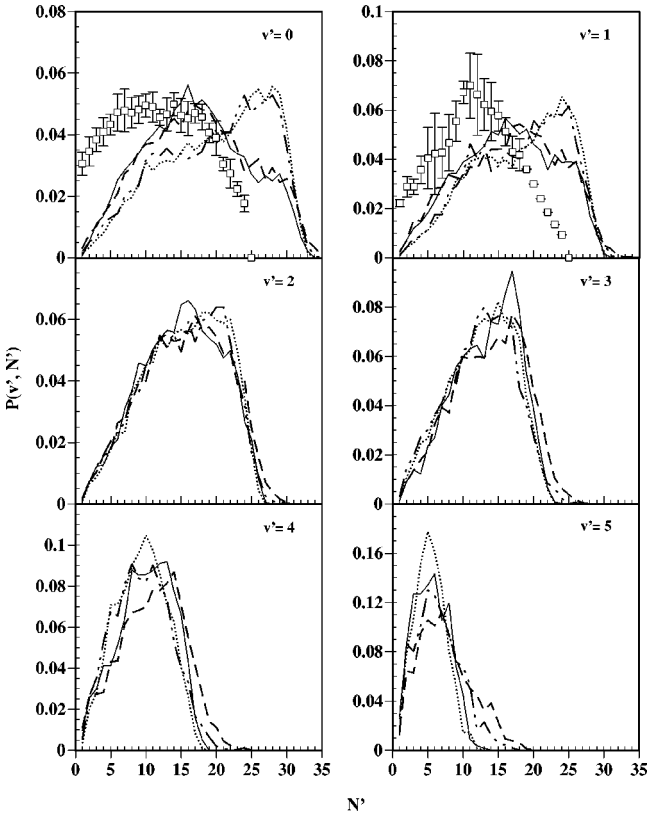


FIG. 2. QCT [—-PES1–0.403 eV, – – PES1-$f(E_T)$, ⋯ PES2–0.403 eV, and — – – – PES2-$f(E_T)$] and experimental (□, Ref. 19) OH($X^2\Pi$, $v'=0-5$) rotational distributions arising from reaction (1) with O($^1D$) generated by photodissociation of $N_2O$ at 193 nm. Typical statistical errors (one standard deviation) for QCT results are about 10%.

tants are used (Table III). Very similar vibrational and rotational distributions are obtained for both conditions, although a slightly higher internal excitation of OH($X\,^2\Pi$, $v'=4-6$) is observed for $f(E_T)$. This is probably due to the tail of high collision energies included in $f(E_T)$. When PES1 and PES2 are compared the results are more similar than those stated above for $E_T=0.212$ eV (Table III). Vibrational populations and rotational populations (mainly for $v'=2-4$) are in general very close to those of PES1, while a higher rotational excitation at $v'=0-1$ is found for PES2. The QCT $P(v'=0)/P(v'=1)$ population ratios for both PES fall between the two experimental values reported[18,19] (Table III and Fig. 1). The QCT rotational distributions for both PES at $v'=0-1$ are more excited than the experimental distributions[19] (Fig. 2).

Hence, the QCT calculations on PES1 and PES2 reproduce quite well the experimental data obtained for the OH($X\,^2\Pi$) product vibrational distribution and rotational distributions for $v'=2-4$ at different initial conditions. However, poorer results are obtained when comparing the rotational distributions for $v'=0-1$ (particularly at $E_T=0.403$ eV), the QCT distributions being more excited than the experimental ones, especially for PES2. The connection of these results with the ability of PES1 and PES2 to describe the microscopic reaction mechanisms of reaction (1) is discussed in Sec. III D.

### C. Stereodynamics

Polarized Doppler-resolved LIF spectroscopy was used to study the stereodynamics of reaction (1) considering the OH($X\,^2\Pi_{3/2}, v'=0, N'=5, \Pi(A')$), OH($X\,^2\Pi_{3/2}, v'=0, N'=5, \Pi(A'')$), OH($X\,^2\Pi_{3/2}, v'=0, N'=8, \Pi(A')$) and OH($X\,^2\Pi_{3/2}, v'=4, N'=8$) quantum states.[22–26] In all cases the reaction was initiated by photodissociation of $N_2O$ at 193 nm. Indistinguishable $\mathbf{kk}'$ differential cross sections (DCS) were found for the two $\Lambda$ doublet components of the OH($X\,^2\Pi_{3/2}, v'=0, N'=5$) product, both displaying forward and backward peaks and a slightly greater tendency towards the backward hemisphere (forward–backward ($f/b$) ratio equal to 0.86 and $\langle \mathbf{kk}' \rangle = 95.5°$).[25] Similar results were observed for the OH($X\,^2\Pi_{3/2}, v'=0, N'=8, \Pi(A')$) state.[25] Regarding the $\mathbf{k}'\mathbf{j}'$ correlation, a preferential $\mathbf{j}' \perp \mathbf{k}'$ polarization was found for the OH($X\,^2\Pi_{3/2}, v'=0, N'=5, \Pi(A')$) state, in contrast with the near isotropic angular distribution of the $\Pi(A'')$ state.[24] Furthermore, the relative translational energy was nearly conserved for OH($X\,^2\Pi_{3/2}, v'=0, N'=5, 8$) ($\langle E_T' \rangle = 0.51$ eV for $N'=5$) and a high internal excitation of the $CH_3$ coproduct was suggested.[24–26] The OH($X\,^2\Pi_{3/2}, v'=4, N'=8$) product showed different behavior, displaying forward and backward peaks and exhibiting a slightly larger tendency towards the forward hemisphere ($f/b=1.03$ and $\langle \mathbf{kk}' \rangle = 86.8°$), while a trend to convert the remaining energy of the process into translational energy instead of $CH_3$ internal energy was also reported ($\langle E_T' \rangle = 0.25$ eV).[25]

The phase space theory (PST) was used in the same contribution[25] to describe the relative translational energy distributions of products ($P(E_T')$) for the OH($X\,^2\Pi_{3/2}, v'=0, N'=5$) and OH($X\,^2\Pi_{3/2}, v'=4, N'=8$) channels. The experimental $P(E_T')$ distribution for OH($X\,^2\Pi_{3/2}, v'=0, N'=5$) was well fitted using an unconstrained PST model, assuming a reaction probability equal to one for each impact parameter ($b$) with $b \leqslant b_{\max}$. This result came out from the very small changes found in the PST results when different values of $b$ were considered. However, when the PST calculations were applied to OH($X\,^2\Pi_{3/2}, v'=4, N'=8$) important differences between the results obtained for different values of $b$ were found. Thus, only PST calculations at high $b$ values reproduced the experimental $P(E_T')$ distribution for OH($X\,^2\Pi_{3/2}, v'=4, N'=8$).

The $\mathbf{kk}'$ DCS and $P(E_T')$ distributions for reaction (1) leading to OH($v'=0, N'=5$) and OH($v'=4, N'=8$) were calculated applying the QCT method on PES1 and PES2, using both the mean $E_T$ value (0.403 eV) and $f(E_T)$. To minimize statistical errors in these state-specific QCT calculations, the stereodynamics properties were calculated for bins of five rotational quantum states instead of a selected state. The quantum states OH($v'=0, N'=3-7$) and OH($v'=4, N'=6-10$) were considered in the calculations. The state-specific QCT and experimental data concerning the $\mathbf{kk}'$ DCS and the $E_T'$ distributions are shown in Figs. 3 and 4, respectively. Moreover, the PST $E_T'$ distributions reported in Ref. 25 that best fitted the measured distributions are also included in Fig. 4.

As can be deduced from Figs. 3 and 4, a good agreement

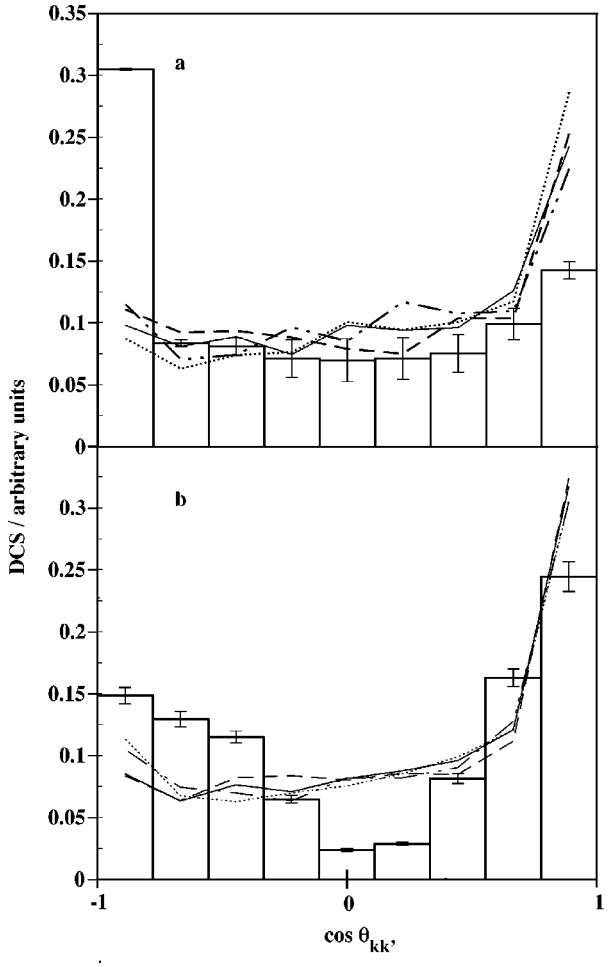


FIG. 3. QCT [—- PES1–0.403 eV, – – PES1-$f(E_T)$, ⋯ PES2–0.403 eV, and — – – — PES2-$f(E_T)$] and experimental (histogram, Ref. 25) **kk**′ DCS for: (a) OH($X^2\Pi$, $v'=0$, $N'=5$); (b) OH($X^2\Pi$, $v'=4$, $N'=8$). These molecules arise from reaction (1) with O($^1D$) generated by photodissociation of $N_2O$ at 193 nm. Typical statistical errors (one standard deviation) for QCT results are about 10%. See text.

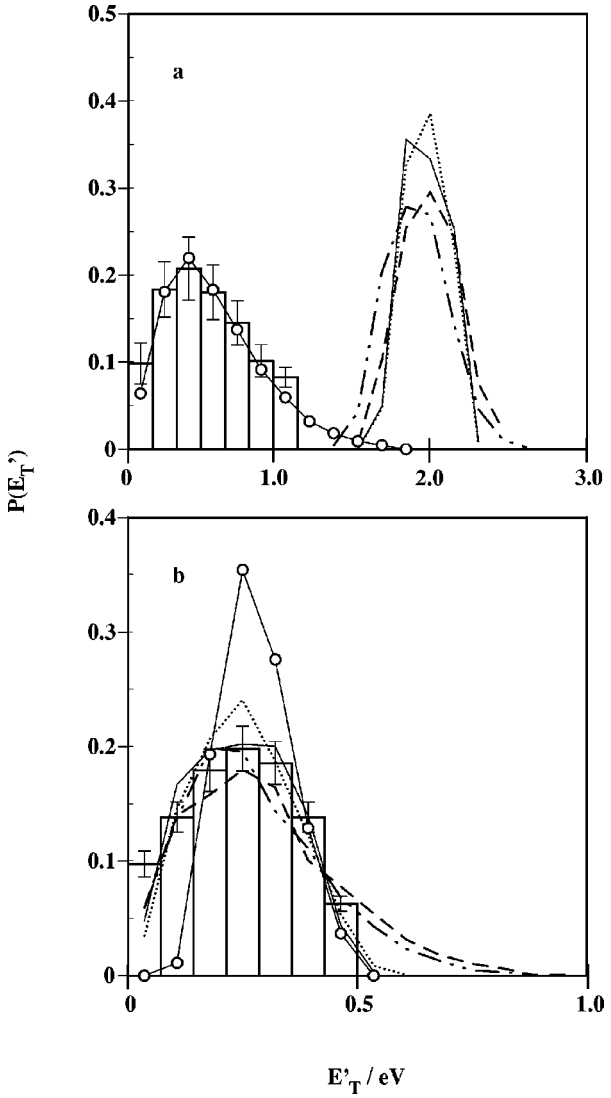


FIG. 4. QCT [—- PES1–0.403 eV, – – PES1-$f(E_T)$, ⋯ PES2–0.403 eV, and — – – — PES2-$f(E_T)$], PST (○, Ref. 25) and experimental (histogram, Ref. 25) $E_T'$ distribution for: (a) OH($X^2\Pi$, $v'=0$, $N'=5$); (b) OH($X^2\Pi$, $v'=4$, $N'=8$). These molecules arise from reaction (1) with O($^1D$) generated by photodissociation of $N_2O$ at 193 nm. Typical statistical errors (one standard deviation) for QCT results are about 10%. See text.

between the QCT calculations and the experimental data of reaction (1) is achieved when the channel leading to vibrationally excited OH molecules is considered. Thus, both the experimental **kk**′ DCS and $P(E_T')$ distribution of the OH($v'=4$, $N'=8$) product are reproduced by the QCT calculations for the two PES studied, when either $E_T=0.403$ eV or $f(E_T)$ are taken into account. Moreover, the $f/b$, $\langle \mathbf{kk}' \rangle$ and $\langle E_T' \rangle$ values are, respectively, within the intervals 1.82–1.98, 70.0°–72.5°, and 0.26–0.31 eV, depending on the PES and the initial conditions. On the other hand, the **kk**′ DCS obtained for OH($v'=0$, $N'=5$) shows a forward peak ($f/b=1.31$–$1.56$ and $\langle \mathbf{kk}' \rangle = 77.5°$–$79.2°$), in contrast to the backward peak found experimentally. The QCT results predict for OH($v'=0$, $N'=5$) a more efficient conversion of energy into final translation than that reported in the experiments. The calculated $\langle E_T' \rangle$ value ranges between 1.91 and 2.00 eV, i.e., it is about four times the experimental one ($\langle E_T' \rangle = 0.51$ eV). The opacity functions leading to OH($v'=0$, $N'=5$) and OH($v'=4$, $N'=8$) channels are quite similar, being flat or slightly decreasing for low and intermediate $b$ values, and then strongly decreasing from $b/b_{max}$ ratio values of about 0.5.

The differences between the QCT and experimental data when the reaction leads to cold OH molecules, such as OH ($v'=0$, $N'=5$), can be understood on the basis of the triatomic model used, which neglects the internal degrees of freedom of the $CH_3$ fragment. The stereodynamics experiments pointed out[22–26] that the less excited the OH molecules arising from reaction (1) the higher the internal excitation displayed in the $CH_3$ coproduct. However, the energy transfer to the methyl fragment, that is particularly important for $v'=0$, cannot be accounted for by the triatomic model. Moreover, the tendency to improve the theoretical reproduction of the experimental behavior of reaction (1) as the excitation of the OH product increases, that was also observed in the study of the OH rovibrational distributions, arises from

the corresponding progressively less energy transfer towards the $CH_3$ fragment that takes place.

In the Doppler-resolved experimental studies, an analysis of the differences between the **kk**′ DCS for OH($v'=0$, $N'=5$) and OH($v'=4$, $N'=8$) was proposed in terms of the lifetime ($t_{\text{complex}}$) and rotational period ($t_r$) of the $CH_3OH$ collision complex, through which reaction (1) is believed to evolve. In those studies, taking into account the QCT and experimental results reported for the $O(^1D)+H_2\rightarrow OH+H$ reaction,[26] the trend towards an increasingly symmetric **kk**′ DCS with increasing vibration in the scattered OH product was interpreted on the basis of an increasing contribution from collisions which involve collision complexes with lifetimes longer than their rotational periods.

Although this tendency was not observed in the present QCT calculations, the mean collision complex lifetime was determined for reactive trajectories leading to OH($v'=0$, $N'=3-7$) and OH($v'=4$, $N'=6-10$). The average rotational periods were calculated using the expression:

$$\langle t_r\rangle=\left\langle \frac{2\pi I}{(2\mu E_T)^{1/2}b}\right\rangle, \tag{5}$$

where $\mu$ is the reduced mass of the reactants, $b$ is the impact parameter, and $I$ is the moment of inertia of the collision complex (average value of the principal moments of inertia of the $(CH_3)OH$ minimum at its equilibrium geometry). The mean rotational periods obtained for the $(CH_3)OH$ collision complex do not appreciably depend on the OH internal energy. They take values around 0.35 ps for PES1 and around 0.25 ps for PES2 at both specific OH states, and they are considerably larger than $\langle t_{\text{complex}}\rangle$ [about 0.1 ps for both PES and OH quantum states, taking into account all reactive trajectories evolving through insertion (see also Sec. IV)].

An **l**→**l**′ angular momentum transformation trend was observed for the OH($v'=0$, $N'=3-7$) and OH($v'=4$, $N'=6-10$), as expected for a reaction with **H**–**L**–**H** (heavy–light–heavy) kinematics. The two vector angular distributions (DCS) **kj**′, **k**′**j**′, and **l**′**j**′ were also characterized in the QCT calculations for these state-selected products. Similar results were obtained for both PES considered, irrespective of whether $E_T=0.403$ eV or $f(E_T)$ is used in the calculations. For both OH quantum states, the **kj**′ DCS are symmetrically distributed around 90° (as they must be) and exhibit a maximum at this angle. The **k**′**j**′ distributions must also be symmetrical, as shown by the calculation, but only the distribution for OH($v'=4$, $N'=6-10$) presents a maximum at 90°.

### D. Microscopic reaction mechanism

A detailed analysis of the temporal evolution of the interatomic distances and PES energy for the reactive trajectories of reaction (1) was performed, employing the QCT method on PES1 and PES2 for $E_T=0.403$ eV and $f(E_T)$. From this analysis, the reactive trajectories were classified into three groups: (a) trajectories leading directly to $OH+(CH_3)$ products without passing through a methanol-like structure (abstraction mechanism); (b) trajectories evolving through geometrical arrangements close to the $(CH_3)OH$ minimum and with the collision complex dissociating fastly (insertion/fast elimination mechanism); (c) trajectories passing close to the $(CH_3)OH$ minimum but with the collision complex dissociating more slowly than in (b) (insertion/slow elimination mechanism).

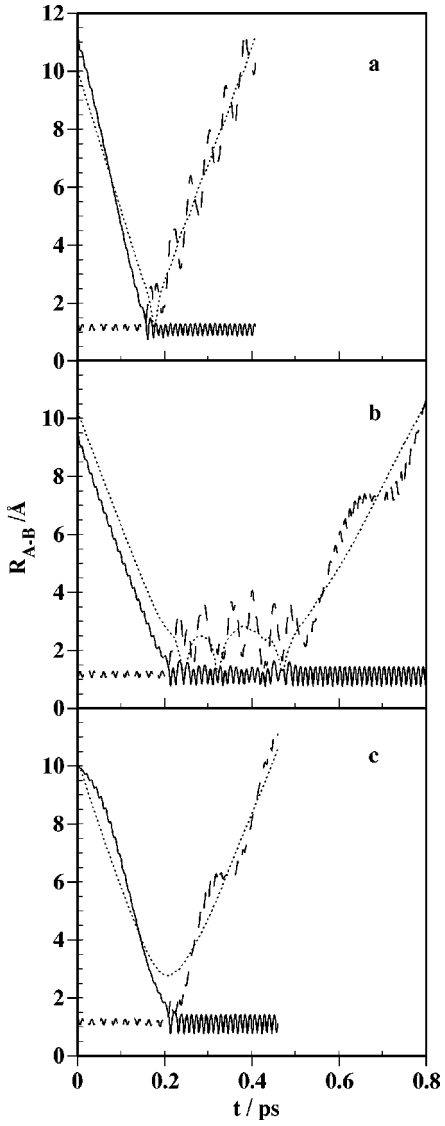


FIG. 5. Evolution of the interatomic distances (—$R_{OH}$, – – $R_{H-(CH3)}$, and ⋯ $R_{O-(CH3)}$) for representative reactive trajectories: (a) insertion/fast elimination; (b) insertion/slow elimination; (c) abstraction.

The typical evolution of the $R_{O-H}$, $R_{H-(CH3)}$, and $R_{O-(CH3)}$ interatomic distances for the three different types of reactive trajectories is given in Fig. 5. The relative contributions of the three microscopic mechanisms to the global reactivity for the PES and $E_T$ conditions studied are given in

TABLE IV. Microscopic mechanisms yields.

| | PES1 | | PES2 | |
|---|---|---|---|---|
| Mechanism | $E_T=0.403$ eV | $f(E_T)$ | $E_T=0.403$ eV | $f(E_T)$ |
| Insertion/fast elimination | 0.47 | 0.47 | 0.49 | 0.49 |
| Insertion/slow elimination | 0.52 | 0.51 | 0.50 | 0.49 |
| Abstraction | 0.01 | 0.02 | 0.01 | 0.02 |

TABLE V. Vibrational populations and average rotational levels of OH($X\ ^2\Pi$) arising from the different microscopic mechanisms found for the O($^1D$) $+CH_4 \rightarrow OH+CH_3$ reaction.[a]

| | | $P(v')$ and $\langle N' \rangle_{v'}$ | | | | | | |
|---|---|---|---|---|---|---|---|---|
| System | Mechanism | $v'=0$ | $v'=1$ | $v'=2$ | $v'=3$ | $v'=4$ | $v'=5$ | $v'=6$ |
| | Insertion/ | 0.11 | 0.10 | 0.11 | 0.11 | 0.05 | 0.006 | |
| | fast elimination | (15.4±0.5) | (15.8±0.5) | (14.9±0.5) | (13.3±0.4) | (10.2±0.4) | (5.6±0.6) | |
| PES1 | Insertion/ | 0.15 | 0.13 | 0.10 | 0.09 | 0.05 | 0.009 | |
| $E_T=0.403$ eV | slow elimination | (17.8±0.5) | (16.9±0.5) | (15.1±0.5) | (13.1±0.4) | (9.6±0.4) | (5.5±0.5) | |
| | Abstraction | 0 | 0 | 0 | $1\times10^{-4}$ | 0.006 | $5\times10^{-4}$ | |
| | | | | | | (8.3±0.7) | | |
| | Insertion/ | 0.10 | 0.10 | 0.11 | 0.10 | 0.05 | 0.01 | $2\times10^{-4}$ |
| | fast elimination | (16.1±0.5) | (15.8±0.5) | (15.5±0.4) | (13.7±0.4) | (11.2±0.4) | (7.8±0.6) | |
| PES1 | Insertion/ | 0.14 | 0.13 | 0.10 | 0.08 | 0.05 | 0.01 | $4\times10^{-4}$ |
| $f(E_T)$ | slow elimination | (18.4±0.5) | (17.3±0.4) | (15.6±0.4) | (13.5±0.4) | (10.4±0.4) | (7.2±0.6) | |
| | Abstraction | 0 | 0 | $1\times10^{-4}$ | 0.003 | 0.01 | 0.002 | $1\times10^{-4}$ |
| | | | | | | (11.5±0.6) | | |
| | Insertion/ | 0.12 | 0.11 | 0.10 | 0.10 | 0.06 | 0.007 | |
| | fast elimination | (18.0±0.4) | (17.0±0.4) | (14.5±0.4) | (12.3±0.3) | (9.3±0.3) | (5.1±0.5) | |
| PES2 | Insertion/ | 0.15 | 0.13 | 0.10 | 0.08 | 0.03 | 0.004 | |
| $E_T=0.403$ eV | slow elimination | (21.7±0.4) | (19.2±0.4) | (16.3±0.4) | (13.2±0.3) | (9.3±0.4) | (5.8±0.6) | |
| | Abstraction | 0 | 0 | 0 | $2\times10^{-4}$ | 0.003 | $2\times10^{-4}$ | |
| | | | | | | (9.8±0.9) | | |
| | Insertion/ | 0.11 | 0.11 | 0.11 | 0.09 | 0.06 | 0.008 | |
| | fast elimination | (17.5±0.5) | (16.6±0.4) | (14.3±0.4) | (12.1±0.4) | (9.3±0.3) | (6.7±0.7) | |
| PES2 | Insertion/ | 0.14 | 0.12 | 0.10 | 0.08 | 0.04 | 0.005 | |
| $f(E_T)$ | slow elimination | (21.3±0.5) | (19.2±0.5) | (16.1±0.4) | (13.1±0.4) | (9.6±0.4) | (6.8±0.9) | |
| | Abstraction | 0 | 0 | $3\times10^{-4}$ | 0.001 | 0.008 | 0.007 | |
| | | | | | | (12.0±0.9) | (6.2±0.5) | |

[a]For each mechanism and vibrational level, the first value given corresponds to the vibrational population normalized with respect to the sum over all the mechanisms and the second one, appearing in parentheses, is the average rotational level. QCT errors correspond to one standard deviation.

Table IV. The contribution of the abstraction mechanism is negligible in all cases, as it only accounts for around 1% to 2% of the global reactivity. In a previous study,[19] it was observed that the contribution of this mechanism increased with $E_T$, as expected. Thus, for PES1 3.5% and 8.3% of the global reactivity corresponds to abstraction at $E_T=0.6$ and 0.8 eV, respectively. Both the microscopic mechanisms involved in the insertion process present yields close to 50%.

The minimal value of the PES energy reached by each reactive trajectory was analyzed to characterize the PES regions explored (the PES energies at the equilibrium geometries of reactants, $OH+(CH_3)$ products and $(CH_3)OH$ minimum are, respectively, $-4.79$, $-6.47$, and $-10.56$ (PES1) and $-10.54$ (PES2) eV, where the zero of energy corresponds to $O(^1D)+H+(CH_3)$). All abstraction trajectories evolve from reactants to products with a minimum PES energy higher than $-7.0$ eV. Almost all the remaining trajectories (insertion mechanisms) take minimal energy values below $-9.0$ eV (70%–80% of them with minimal energies lower than $-10.0$ eV).

In mechanisms (b) and (c) the insertion process initially takes place passing through $O–H–(CH_3)$ arrangements and evolving further to $H–O–(CH_3)$ geometries thanks to the $O–H–(CH_3)$ bending motion, as may be expected from the shape of the analytical PES. Reactive trajectories classified as (c) present a wide interval of $t_{complex}$, ranging from 0.04 ps (see below) to 2.2 ps with an average value of 0.2 or 0.3 ps, respectively, depending on whether PES1 or PES2 is considered. Most $t_{complex}$ are considerably lower than the experimental value (0.8 ps,[29] although it was not determined whether the O($^1D$) was thermalized before reaction). The average lifetime (3–5 ps) obtained from the corresponding half collision reaction,[20,21] carried out by photolysis of the $O_3 \bullet CH_4$ van der Waals complex, can not be compared with the bimolecular data, due to the different reaction conditions explored.

The QCT average collision complex lifetime obtained here should be considered as a lower limit of the theoretical value which would result if all the degrees of freedom of the $CH_3$ fragment were explicitly accounted for. On the other hand, when the $t_{complex}$ values were analyzed for all reactive trajectories, a gap of lifetime values was observed between 0.02 and 0.04 ps. For reactive trajectories which present a collision complex with a lifetime greater than 0.04 ps, at least one O–H stretching motion was displayed before dissociation. The decomposition of a collision complex evolving without any O-H stretching motion was produced in reactive trajectories with $t_{complex}$ below 0.02 ps. This feature was used here to distinguish between the insertion/fast elimination and insertion/slow elimination mechanisms.

The dynamics properties of the microscopic reaction mechanisms were also studied. The corresponding OH vibrational distributions and the average rotational levels are shown in Table V. The vibrational populations for insertion/fast elimination are essentially constant (around 0.1) in the $v'=0-3$ range and decrease above $v'=3$ ($\langle f'_V \rangle = 0.43 - 0.44$), while they decrease monotonically with $v$' for insertion/slow elimination ($\langle f'_V \rangle = 0.37 - 0.40$). A highly inverted vibrational distribution peaking at $v'=4$ ($\langle f'_V \rangle$

$=0.75-0.85$) occurs in the case of the abstraction mechanism. The insertion/fast elimination yields less rotationally excited OH($X\,^2\Pi$, $v'=0-1$) molecules than the insertion/slow elimination, while the rotational distributions for $v'=2-6$ become more similar as $v'$ increases ($\langle f_R'\rangle=0.20-0.22$ and $\langle f_R'\rangle=0.24-0.31$, respectively). The calculations did not give enough reactive trajectories to justify conclusions about the rotational distributions arising from abstraction ($\langle f_R'\rangle=0.07-0.14$). However, for its most populated vibrational level ($v'=4$) the rotational distribution seems to be similar to those found for reactive trajectories evolving through insertion.

The opacity functions [reaction probability ($P(b)$) vs $b$] are comparable for the two insertion mechanisms: They are almost flat within the $b/b_{\max}=0-0.5$ range, and then monotonically decrease to zero at $b/b_{\max}=1$. Reactivity at high impact parameters is favored for the abstraction mechanism, especially for PES1. Concerning the two vector correlations, the $\mathbf{kk}'$ angular distributions for the three microscopic mechanisms are essentially forward, mostly for abstraction [$f/b=5.1-8.5$ (stripping)]. This can be understood by considering the different shapes of the opacity functions. The $\mathbf{kk}'$ angular distribution for insertion/fast elimination is somewhat more forward ($f/b=2.1-2.6$) than that for insertion/slow elimination ($f/b=1.1-2.3$). The OH rotational angular momentum $\mathbf{j}'$ tends to be perpendicular to both $\mathbf{k}$ and $\mathbf{k}'$, with broad symmetrical distributions around 90°.

The influence of $t_{\text{complex}}$ on the rovibrational distributions for insertion/slow elimination was also analyzed. For reactive trajectories with $t_{\text{complex}}$ greater than 0.07 ps there are few differences in the OH rovibrational distributions. However, when $t_{\text{complex}}$ in the 0.04–0.07 ps range are considered (they only correspond to about 25% and 5% of the total slow elimination reactive trajectories, respectively, for PES1 and PES2), some differences with respect to the remaining ones ($t_{\text{complex}}\geqslant 0.07$ ps) are observed. Thus, the vibrational distribution is more excited (even it is inverted for PES2) and the rotational distributions of $v'=0-1$ are somewhat less excited, especially for PES1, resembling some of the features of the insertion/fast elimination mechanism.

From the different features established in the QCT calculation for the three microscopic mechanisms, some points of connection can be inferred between the present results and previous experimental data on the reaction mode. From LIF measurements of the OH rovibrational distribution,[15,18,19] it was suggested that there are two predominant mechanisms involved in reaction (1): Insertion/fast elimination and insertion/slow elimination. The reactive behavior experimentally suggested for the fast elimination mechanism has been reproduced theoretically using both PES1 and PES2. This mechanism yields vibrationally and rotationally excited OH molecules. The analytical triatomic PES considered, however, clearly fail if the experimental and theoretical properties of the slow elimination mechanism are compared. Although less vibrational excitation has been found theoretically for insertion/slow elimination than for insertion/fast elimination, its calculated vibrational distribution is still hotter than that determined experimentally.[15,18,19] Furthermore, the QCT calculations for insertion/slow elimination yield highly rotationally excited OH molecules, while colder rotational distributions are expected for this type of reaction mode.[15,18,19] On the other hand, the QCT yields for the two insertion mechanisms deviate from the experimentally obtained. Thus, in Refs. 15 ($O_3$ at 248 nm) and 19 ($N_2O$ at 193 nm) it was found that the insertion/slow elimination mechanism only contributed to $v'=0$ (18% and 17%, respectively) and $v'=1$ (6% and 2%, respectively), while the QCT calculations show that about 50% of the insertion mechanism comes from the slow elimination process.

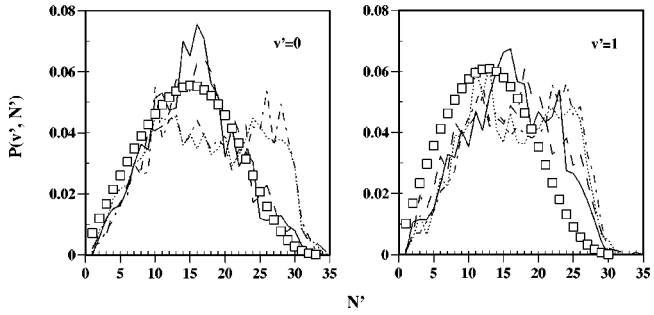


FIG. 6. QCT [—- PES1–0.403 eV, – – PES1-$f(E_T)$, ⋯ PES2–0.403 eV, and — – – — PES2-$f(E_T)$] and experimental (□, Ref. 19) OH($X^2\Pi$, $v'=0$-1) rotational distributions arising from the fast elimination mechanism of reaction (1), when $O(^1D)$ is generated by photodissociation of $N_2O$ at 193 nm. Typical statistical errors (one standard deviation) for QCT results are about 10%.

The discrepancies between the QCT and experimental results, mainly observed for $v'=0-1$, may be understood as a consequence of the triatomic model used in the calculation, as it was already mentioned in Sec. III C. This simplification does not allow to describe the energy transfer to the methyl fragment. The QCT calculations, however, reproduce quite satisfactorily the experimental data involving $v'=2-4$. This is due to the weak influence of the triatomic model on the proper description of the insertion/fast elimination mechanism. Even the experimental rotational distributions arising from this mechanism for $v'=0-1$[15,18,19] (high-$N'$ component of the experimental rotational distributions) show a reasonably good agreement with the QCT results (Fig. 6).

Regarding the abstraction mechanism also found in the QCT study, its negligible contribution to the reactivity (restricted to high $v'$ levels of the OH product) is consistent with the lack of experimental evidence from $OH(X\,^2\Pi_{3/2}, v'=0-4)$ LIF measurements[12,15,18,19] for the involvement of a third reaction mode. However, in a recent experimental study of the half collision $O_3\bullet CH_4$ reaction at 248 nm,[21] the presence of an abstraction mechanism along with the two possible insertion mechanisms mentioned above was established. Nevertheless, this mechanism was assigned to a rebound abstraction reaction mode yielding cold OH products, in contrast to the stripping behavior obtained in the QCT calculations for the abstraction mechanism. On the other hand, the low-$N'$ component of the OH($v'=0-1$) rotational distributions assigned to the abstraction mechanism in the half collision experiment does not seem to appear either in the experimental measurements or in the QCT calculations arising from reaction (1). This discrepancy between

the calculated and experimental results can be explained in terms of the different initial conditions involved in the half collision experiment with respect to the bimolecular reaction simulated in the QCT calculations.

To improve the comparison of the half collision experiment, additional QCT calculations were performed at zero initial impact parameter. Few changes with respect to the standard calculation with an initial distribution of impact parameters were observed regarding the OH vibrational and rotational distributions. The vibrational distribution was somewhat more excited and the rotational distributions for $v'=0-1$ slightly colder. The main differences appear when comparing the two vector angular correlations. The $\mathbf{kk}'$ distribution is strongly backward and the $\mathbf{l}'\mathbf{j}'$ distribution is strongly antiparallel (instead of being quite broad). The $\mathbf{l}'\mathbf{j}'$ result is a consequence of the very small value of the total angular momentum ($\mathbf{l}'+\mathbf{j}'$). Nevertheless, the abstraction branching ratio is still very small (about 1%) and this mechanism still produces internally excited OH molecules with an inverted vibrational distribution, in contrast to the half collision experiments. The persistence of this disagreement between the QCT and half-collision experimental data indicates that aspects other than the initial total angular momentum, e.g., the initial geometry, should be considered in comparisons with this experiment.

## IV. SUMMARY AND CONCLUSIONS

A previously reported PES (PES1) and a barrierless new PES (PES2), both built from *ab initio* information, were considered to study in the framework of a triatomic model (methyl group treated as a pseudoatom) the dynamics, stereodynamics and microscopic mechanism of the $O(^1D)+CH_4\rightarrow OH+CH_3$ reaction by means of the QCT method. As the fully *ab initio* based PES1 presents a small barrier and the experimental measurements of the rate constant suggest that there is no activation energy for this reaction, special care was taken to obtain a barrierless PES. The new PES accurately reproduces the experimental rate constant of the global (including the $OH+CH_3$ and $CH_3O+H$ reaction channels) $O(^1D)+CH_4$ reaction and the branching ratio of the $OH+CH_3$ channel in the 200–350 K range.

The QCT calculations on PES1 and PES2 were mainly performed at the initial relative translational energy of the experiments where reaction (1) is initiated by photolysis of $N_2O$ at 193 nm ($\langle E_T\rangle=0.403$ eV), although the collision energy obtained from the photodissociation of $O_3$ at 248 nm ($\langle E_T\rangle=0.212$ eV) was also considered. The results obtained regarding the rovibrational distribution of the $OH(X\,^2\Pi)$ molecules, the two vector correlations of the $OH+CH_3$ products, and the features of the microscopic mechanisms involved in reaction (1) show a small dependence on whether PES1 or PES2 and the full translational energy distribution of reactants or its average value are considered.

Good agreement between QCT and experimental results was obtained for the OH vibrational populations and for the OH rotational populations for the $v'\geqslant 2$ vibrational levels, while the rotational distributions for $v'=0-1$ are more excited than in the experiment. At 0.403 eV the experimental $\mathbf{kk}'$ angular distribution and translational energy distribution of products are properly reproduced for the state-specific channel leading to $OH(v'=4,\ N'=8)$. The agreement with the experiment, however, is poorer for $OH(v'=0,\ N'=5)$, particularly for the $E_T'$ distribution.

The analysis of the microscopic reaction mechanism at 0.403 eV shows that the reaction takes place almost exclusively through the insertion of the $O(^1D)$ atom into a C–H bond to yield $CH_3OH$ collision complexes (abstraction (stripping) mechanism only contributes to 1%–2% of the global reactivity). The dissociation of the collision complex can be displayed following a fast elimination or a slow elimination process. These two insertion like reaction modes were also suggested from the experiments as the most important ones for the dynamics. The QCT reactive behavior for insertion/fast elimination trajectories yielding vibrationally and rotationally excited OH molecules agrees with the experimental information available. However, more internally excited OH molecules are found in the QCT calculations for the insertion/slow elimination mechanism with respect to what has been obtained experimentally. This discrepancy between theory and experiment regarding the insertion/slow elimination reaction mode can be understood as a consequence of the triatomic model used. The excitation of the $CH_3$ coproduct that ought to yield this kind of microscopic mechanism cannot be described by this model.

In spite of the relative simplicity of the triatomic modeling, many aspects of the $O(^1D)+CH_4\rightarrow CH_3+OH$ reaction can be satisfactorily described by this approach. The triatomic modeling may be considered as an initial step in the theoretical treatment of the dynamics of polyatomic systems from which much can be learned.

## ACKNOWLEDGMENTS

This work was supported by the ''Dirección General de Enseñanza Superior'' of the Spanish Ministry of Education and Culture through the DGES projects PB95-0598-C02-01 and -02, and PB98-1209-C02-01 and -02. J.H. thanks the CIRIT from the ''Generalitat de Catalunya'' (Autonomous Government of Catalonia) for a predoctoral research grant. The authors are also grateful to the ''Generalitat de Catalunya'' (Ref. 1998SGR 00008), to the ''Center de Supercomputació i Comunicacions de Catalunya ($C^4$- CESCA/CEPBA)'' for computer time made available, and to Dr. John C. Stephenson (NIST, Gaithersburg (USA)) for sending us a copy of his manuscript.

[1] J. R. Wiesenfeld, Acc. Chem. Res. **15**, 110 (1982).
[2] P. Warneck, *Chemistry of the Natural Atmosphere* (Academic, San Diego, 1988).
[3] E. B. Burnett and C. R. Burnett, J. Atmos. Chem. **21**, 13 (1995).
[4] M. W. Chase, Jr., C. A. Davies, J. R. Downey, Jr., D. J. Frurip, R. A. McDonald, and A. N. Syverud, J. Phys. Chem. Ref. Data **14**, Suppl. 1 (1985).
[5] R. Atkinson, D. L. Baulch, R. A. Cox, R. F. Hampson, Jr., J. A. Kerr, M. J. Rossi, and J. Troe, J. Phys. Chem. Ref. Data **28**, 191 (1999).
[6] M. González, J. Hernando, J. Millán, and R. Sayós, J. Chem. Phys. **110**, 7326 (1999), and references therein.
[7] J. J. Lin, S. Harich, Y. T. Lee, and X. Yang, J. Chem. Phys. **110**, 10821 (1999).
[8] W. Hack and H. Thiesemann, J. Phys. Chem. **99**, 17364 (1995).
[9] S. Satpayal, J. Park, R. Bersohn, and B. Katz, J. Chem. Phys. **91**, 6873 (1989).

[10] Y. Matsumi, K. Tonokura, Y. Inagaki, and M. Kawasaki, J. Phys. Chem. **97**, 6816 (1993).
[11] R. A. Brownsword, M. Hillenkamp, P. Schmiechen, H.-R. Volpp, and H. P. Upadhyaya, J. Phys. Chem. **102**, 4438 (1998).
[12] A. C. Luntz, J. Chem. Phys. **73**, 1143 (1980).
[13] P. M. Aker, J. J. A. O'Brien, and J. J. Sloan, J. Chem. Phys. **84**, 745 (1986).
[14] S. G. Cheskis, A. A. Iogansen, P. V. Kulakov, I. Yu. Razuvaev, O. M. Sarkisov, and A. A. Titov, Chem. Phys. Lett. **155**, 37 (1989).
[15] C. R. Park and J. R. Wiesenfeld, J. Chem. Phys. **95**, 8166 (1991).
[16] Y. Rudich, Y. Hurwitz, G. J. Frost, V. Vaida, and R. Naaman, J. Chem. Phys. **99**, 4500 (1993).
[17] M. González, J. Hernando, R. Sayós, M. P. Puyuelo, P. A. Enríquez, J. Guallar, and I. Baños, Faraday Discuss. **108**, 453 (1997).
[18] S. Wada and K. Obi, J. Phys. Chem. A **102**, 3481 (1998).
[19] M. González, M. P. Puyuelo, J. Hernando, R. Sayós, P. A. Enríquez, J. Guallar, and I. Baños, J. Phys. Chem. A **104**, 521 (2000).
[20] R. D. van Zee and J. C. Stephenson, J. Chem. Phys. **102**, 6946 (1995).
[21] C. C. Miller, R. D. van Zee, and J. C. Stephenson (in preparation).
[22] M. Brouard, S. P. Duxon, and J. P. Simons, Isr. J. Chem. **34**, 67 (1994).
[23] M. Brouard and J.P. Simons, in *The Chemical Dynamics and Kinetics of Small Radicals*, Part II, edited by K. Liu and A. Wagner (World Scientific, Singapore, 1995), p. 795.
[24] M. Brouard, H. M. Lambert, J. Short, and J. P. Simons, J. Phys. Chem. **99**, 13571 (1995).
[25] M. Brouard, H. M. Lambert, C. L. Russell, J. Short, and J. P. Simons, Faraday Discuss. **102**, 179 (1995).
[26] J. P. Simons, J. Chem. Soc., Faraday Trans. **93**, 4095 (1997).
[27] T. Suzuki and E. Hirota, J. Chem. Phys. **98**, 2387 (1993).
[28] R. Schott, J. Schlütter, M. Olzmann, and K. Kleinermanns, J. Chem. Phys. **102**, 8371 (1995).
[29] C.-L. Lin and W. B. DeMore, J. Phys. Chem. **77**, 863 (1973).
[30] S. P. Walch, J. Chem. Phys. **98**, 3163 (1993).
[31] H. Arai, S. Kato, and S. Koda, J. Phys. Chem. **98**, 12 (1994).
[32] M. González, J. Hernando, I. Baños, and R. Sayós, J. Chem. Phys. **111**, 8913 (1999).
[33] J. N. Murrell, S. Carter, S. C. Farantos, P. Huxley, and A. J. C. Varandas, in *Molecular Potential Energy Surfaces* (Wiley, New York, 1984).
[34] M. Gilibert, A. Aguilar, M. González, F. Mota, and R. Sayós, J. Chem. Phys. **97**, 5542 (1992).
[35] M. González, J. Hijazo, J. J. Novoa, and R. Sayós, J. Chem. Phys. **105**, 10999 (1996).
[36] M. González, J. Hijazo, J. J. Novoa, and R. Sayós, J. Chem. Phys. **108**, 3168 (1998).
[37] R. Sayós, J. Hijazo, M. Gilibert, and M. González, Chem. Phys. Lett. **284**, 101 (1998).
[38] R. Sayós, J. Hernando, J. Hijazo, and M. González, Phys. Chem. Chem. Phys. **1**, 947 (1999).
[39] M. González and R. Sayós, DIATOMFIT (unpublished program).
[40] R. Sayós and M. González, SM3FIT (unpublished program).
[41] R. N. Porter and L. M. Raff, in *Dynamics of Molecular Collisions*, Part B, edited by W.H. Miller (Plenum, New York, 1976), p. 1.
[42] D. G. Thuhlar and J. T. Muckerman, in *Atom-Molecule Collision Theory: A Guide for the Experimentalist*, edited by R. B. Bernstein (Plenum, New York, 1979), p. 505.
[43] H. R. Mayne, Int. Rev. Phys. Chem. **10**, 107 (1991).
[44] R. Sayós and M. González, TRIQCT (unpublished program).
[45] R. Steckler, Y.-Y. Chuang, E. L. Coitiño *et al.*, POLYRATE version 7.0, University of Minnesota, Minneapolis, 1996.
[46] P. Felder, B.-M. Haas, and J. R. Huber, Chem. Phys. Lett. **186**, 177 (1991).
[47] L. L. Springsteen, S. Satpayal, Y. Matsumi, L. M. Dobeck, and P. L. Houston, J. Phys. Chem. **97**, 7239 (1993).